Cosmological Probes of Lepton Parity Freeze-in Dark Matter: $\Delta N_{\rm eff}$ & Gravitational Waves

Ernest Ma,¹ Partha Kumar Paul⁰,^{2,*} and Narendra Sahu⁰, †

In the canonical type-I seesaw mechanism for neutrino masses, a residual symmetry known as lepton parity: $(-1)^L$, remains preserved. Introducing a Majorana fermion S with even lepton parity renders it naturally stable, making it a viable dark matter (DM) candidate. The addition of a lepton parity odd singlet scalar σ allows for the coupling $NS\sigma$, where N is the right-handed neutrino. If S is not thermalized, then DM relic can be produced in two distinct ways: (i) for reheating temperature, $T_{\rm rh} > m_N$, dominantly through the decay of N ($N \to S\sigma$), and (ii) for $T_{\rm EW} < T_{\rm rh} \ll m_N$, via standard model Higgs (h) decay ($h \to SS$ at one loop). If the $\sigma - h$ quartic coupling is large, then it can lead to a strong first-order electroweak phase transition even if $\langle \sigma \rangle = 0$. Alternatively, if $\sigma - h$ coupling is small, then σ can freeze out with a larger abundance, and hence its decay ($\sigma \to S\nu$) at late epochs can give rise to additional relativistic degrees of freedom ($\Delta N_{\rm eff}$). Thus, the framework gives a viable DM with mass range varying from MeV to TeV and leaves observable imprints, via gravitational waves and $\Delta N_{\rm eff}$, which offer complementary probes, potentially detectable in future gravitational wave and CMB experiments.

I. INTRODUCTION

To accommodate naturally small Majorana neutrino masses, the standard model (SM) of quarks and leptons is routinely extended to include three singlet right-handed neutrinos (RHN) N with large Majorana masses, implementing thus the well-known type-I seesaw mechanism [1-4]. The resulting model conserves lepton parity $(-1)^L$, which may be used to define dark parity $(-1)^{(L+2j)}$ [5]. Suppose a singlet left-handed Majorana fermion S is added with even lepton parity (hence odd dark parity), then it is a dark matter (DM) candidate. To connect it with the SM, a singlet real scalar σ may be added. The case of σ even under lepton(dark) parity has been discussed in two recent papers [6, 7]. The former considers the case where $m_{\sigma}^2 > 0$ [6], resulting in a small vacuum expectation value (VEV), and the latter the case with $m_{\sigma}^2 < 0$ [7], resulting in a large VEV. Here we consider the other possible option, i.e., σ is odd under lepton(dark) parity with no VEV, and study the related phenomenologies beyond the SM.

If we assume a large $\sigma^2 H^\dagger H$ coupling, where H is the SM Higgs doublet, then it enables the appearance of a first-order electroweak phase transition (EWPT) [8, 9] in the early Universe, which results in stochastic gravitational waves. This can give rise to detectable signatures at different gravitational wave experiments. If DM S is not thermalized, then its relic can be obtained from N or Higgs decay, depending on the reheat temperature of the Universe.

Alternately, if $\sigma^2 H^{\dagger} H$ coupling is small, then σ can freeze out with a larger abundance in the early Universe.

The late decay of σ through $\sigma \to S\nu$ channel can give rise to the non-thermal production of light degrees of freedom, $N_{\rm eff}$ as well as DM. In this scenario, if we demand that the DM relic from σ decay is in the correct range, then it results in a larger $\Delta N_{\rm eff}$ which is ruled out by the present CMB experiments. On the other hand if we demand the σ decay produces the observable $\Delta N_{\rm eff}$, then the relic of S remains underabundant. The deficit can be fulfilled through N or H decay, depending on the reheat temperature of the Universe. Thus it gives rise to a complementary probe of the scenario at different cosmic microwave background (CMB) experiments such as DESI [10], Planck [11], ACT [12], Planck+ACT [12], SPT-3G [13], CMB-S4 [14], and CMB-HD [15].

The paper is organized as follows. In section II, we discuss the minimal model in detail. Section III is devoted to discussing the DM phenomenology and its probe at terrestrial experiments when the reheat temperature is large $(T_{\rm rh} > m_N)$. The DM phenomenology with low reheat temperature $(T_{\rm EW} < T_{\rm rh} \ll m_N)$ is discussed in section IV. We finally conclude in section V.

II. MINIMAL MODEL

In the minimal type-I seesaw framework, lepton number is explicitly broken down to a residual lepton parity symmetry $(-1)^L$. By construction, the SM leptons are odd under this residual lepton parity, and we choose the RHN, N, to be also odd under lepton parity. In this work, we extend the minimal type-I seesaw model by introducing a left-handed fermion, S, which carries even lepton parity and is therefore disconnected from the SM sector. This makes S a natural DM candidate. To enable its production in the early Universe, we further introduce a singlet scalar, σ , which is odd under lepton parity with a mass hierarchy as $m_N > m_{\sigma} > m_S$. The relevant La-

¹Department of Physics and Astronomy, University of California, Riverside, California 92521, USA ²Department of Physics, Indian Institute of Technology Hyderabad, Kandi, Telangana-502285, India. (Dated: November 27, 2025)

^{*} ph22resch11012@iith.ac.in

[†] nsahu@phy.iith.ac.in

grangian is then given as

$$\mathcal{L} = \overline{N}i\gamma^{\mu}\partial_{\mu}N - \frac{1}{2}m_{N_{i}}\overline{N_{i}^{C}}N_{i} + \overline{S}i\gamma^{\mu}\partial_{\mu}S - \frac{1}{2}m_{S}\overline{S^{C}}S$$
$$-y_{\alpha i}\overline{L}_{\alpha}\tilde{H}N_{i} - y_{NS}\overline{N_{i}}S\sigma + \text{H.c.} - V(H, \sigma), \tag{1}$$

where $i \in [1, 2], \alpha \in [e, \mu, \tau]$ and the most general scalar potential is given as

$$V(H,\sigma) = -\mu_h^2 H^{\dagger} H + \lambda_h (H^{\dagger} H)^2 + \frac{1}{2} \mu_{\sigma}^2 \sigma^2 + \frac{1}{4} \lambda_{\sigma} \sigma^4 + \lambda_{h\sigma} H^{\dagger} H \sigma^2, \qquad (2)$$

where the Higgs field can be parameterized after electroweak symmetry breaking as $H = \begin{pmatrix} 0 & (h+v_h)/\sqrt{2} \end{pmatrix}$ with v_h being the VEV of the SM Higgs.

Depending on the reheating temperature of the Universe, the DM relic can be realized in two distinct scenarios: i) for reheating temperature, $T_{\rm rh} > m_{N_1}$, and ii) for reheating temperature, $T_{\rm EW} < T_{\rm rh} \ll m_{N_1}$, where m_{N_1} is the mass of lightest RHN N_1 .

Case-i) $T_{\rm rh} > m_{N_1}$: As the $T_{\rm rh}$ is larger than the mass of $\overline{N_1}$, it can be produced abundantly from the thermal bath through the LHN coupling. As such, the out-ofequilibrium decay of N_1 in the early Universe can also give rise to a net lepton asymmetry. Moreover, if the coupling between σ and SM Higgs, $\lambda_{h\sigma}$ is large enough (typically $\lambda_{h\sigma} > 1$), it will trigger a first-order electroweak phase transition (FOEWPT). This will result in stochastic gravitational waves, potentially observable in future GW experiments. Moreover, the freeze-out relic of σ is small. Therefore, any late decay of σ will give a negligible contribution to the DM relic. On the other hand, if $\lambda_{h\sigma}$ (typically $\lambda_{h\sigma} \ll 1$) coupling is small, σ freezes out from the thermal bath with a larger abundance. Its late decay can then contribute to the DM relic density as well as additional relativistic degrees of freedom (d.o.f) $(\Delta N_{\rm eff})$ in the form of light neutrinos. Such a scenario may yield distinctive signatures testable in future CMB experiments. By demanding that $\Delta N_{\rm eff} \lesssim 0.4$, we will show that late decay of σ cannot give rise to the correct relic abundance of S. Thus, irrespective of the values of $\lambda_{h\sigma}$, the contribution of σ to the DM relic is negligible. In this scenario, the relic of DM is dominantly produced by N_1 decay (i.e., $N_1 \to S\sigma$). Even if $h \to SS$ is allowed at one loop, its contribution to S abundance is negligible in comparison to N_1 decay. This is because the production of S from Higgs decay is proportional to y_{NS}^4 , whereas the production of S from N_1 decay is proportional to

Case-ii) $T_{\rm EW} < T_{\rm rh} \ll m_{N_1}$: In this scenario, N_1 cannot be produced from the thermal plasma. However, the DM can be produced from the SM Higgs decay at one loop level. As discussed in the previous paragraph, this scenario also may yield distinctive signatures testable in future CMB and GW experiments. Similar to the above discussion, the contribution of σ decay to DM relic remains negligible.

We will study the phenomenologies of these two scenarios: case-i and case-ii in detail in the following sections.

III. PHENOMENOLOGY WITH $T_{\rm rh} > m_{N_1}$

As discussed above, when the reheat temperature of the Universe, $T_{\rm rh} > m_{N_1}$, the RHNs can be abundantly produced in the early Universe through the NLH coupling. Through the same coupling, the decay of N into the visible sector, LH, can generate a net lepton asymmetry, which then gets converted to baryon asymmetry of the Universe¹ and the details are given in Appendix A. The decay of N to σS can also generate a freeze-in population of DM. In this scenario, depending on the values of $\lambda_{h\sigma}$, two distinct cases for BSM phenomenologies arise: A) large $\lambda_{h\sigma}$ (typically $\lambda_{h\sigma} > 1$), and B) small $\lambda_{h\sigma}$ (typically $\lambda_{h\sigma} \ll 1$).

A. Consequences of Large $\lambda_{h\sigma}$

1. First-order electroweak phase transition (FOEWPT) and stochastic gravitational waves

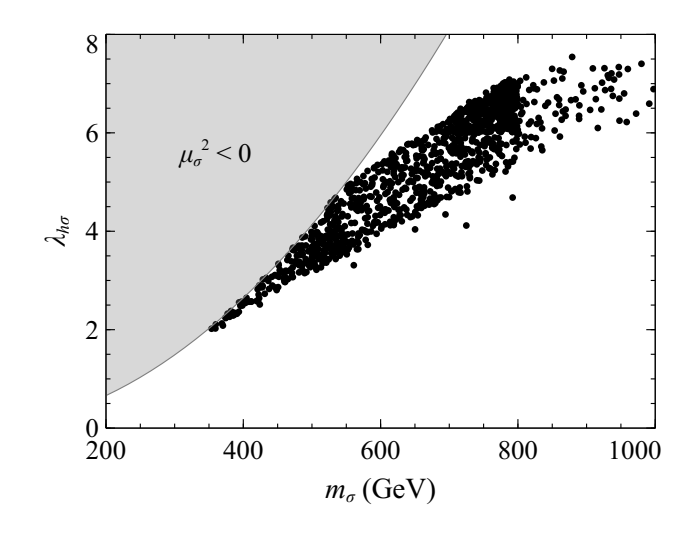


FIG. 1. Parameter space (shown by black dotted points) of first-order EWPT in the plane of $\lambda_{h\sigma}$ vs m_{σ} .

In Eq. 2, we choose $\mu_{\sigma}^{2} > 0$ such that σ does not obtain any VEV and only SM Higgs obtains a VEV: v_{h} . The σ mass gets a contribution from SM Higgs and is given as $m_{\sigma} = \sqrt{\mu_{\sigma}^{2} + \lambda_{h\sigma}v_{h}^{2}}$. The SM Higgs mass is $m_{h} = \sqrt{2}\mu_{h} = 125$ GeV and $\lambda_{h} = 0.129$. The only free parameters in the scalar sector are $\{m_{\sigma}, \lambda_{\sigma}, \lambda_{h\sigma}\}$. The EWPT can be made first-order with the help of this singlet scalar σ through the coupling $\lambda_{h\sigma}$ [8, 9]. Singlet scalar quartic coupling, λ_{σ} does not play any role in the mass of σ , it only contribute to its thermal mass. For

 $^{^1}$ The simultaneous decay of RHNs to visible sector and dark sector can give rise to asymmetric dark matter scenarios, see $\it e.g.$ [16–18]. In the present scenario, $\it S$ being a Majorana fermion, asymmetry in $\it S$ does not exist.

 $\lambda_{\sigma} \sim \mathcal{O}(1)$, the FOPT is weakened. in order to get the largest possible region of FOPT parameter space, we set $\lambda_{\sigma} = 0$. Now the only free parameters determining the FOPT are $\{m_{\sigma}, \lambda_{h\sigma}\}$. The finite temperature effective scalar potential is given in Appendix B. We implement the model in CosmoTransitions [19] and obtain the parameter space of first-order EWPT in the $\lambda_{h\sigma} - m_{\sigma}$ plane as shown in Fig. 1. In the gray shaded region $\mu_{\sigma}^2 < 0$, the

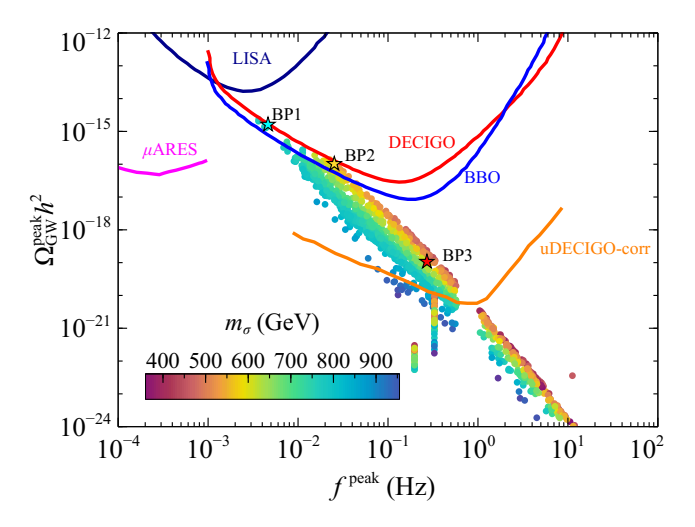


FIG. 2. Peak GW amplitude as a function of peak frequency.

singlet scalar would obtain a non-zero VEV and destabilize the DM due to S-N mixing. Therefore, our region of interest is $\mu_{\sigma}^2 > 0$ and the black points represent the FOEWPT. This restricts the mass and coupling to be in the range $m_{\sigma} \in [350, 1000]$ GeV, $\lambda_{h\sigma} \in [2, 7.5]$. With this large $\lambda_{h\sigma}$, σ will always be in equilibrium and freeze out with negligible relic abundance and will not be a DM candidate, as will be discussed in the next section.

We then compute the peak amplitude and peak frequencies for these FOPT points as shown in Fig. 2. The color code denotes the mass of σ . Sensitivity reaches of different experiments like DECIGO [20], BBO [21], uDECIGO-corr [22, 23], LISA [24], and μ ARES [25] are shown with different color contours. The peak frequency spans from mHz to a few Hz. The amplitude remains in the sensitivities of DECIGO, BBO, and uDECIGO-corr.

| BPs | $m_{\sigma} \; (\text{GeV})$ | λ_{σ} | $T_c \text{ (GeV)}$ | $T_n \text{ (GeV)}$ | α | β/\mathcal{H} |
|-----|------------------------------|--------------------|---------------------|---------------------|----------|---------------------|
| BP1 | 729.1 | 6.63 | 139.3 | 94.45 | 0.024 | 255.79 |
| BP2 | 556.34 | 4.96 | 128.02 | 108.51 | 0.024 | 1219.19 |
| BP3 | 594.86 | 4.61 | 147.39 | 143.86 | 0.0093 | 9838.08 |

TABLE I. Details of the parameters for the three BPs shown in Fig. 2. Here T_c denotes the critical temperature, T_n denotes the nucleation temperature, α is the strength of FOPT defined as the ratio of vacuum energy density to radiation energy density, β represents the inverse duration of phase transition.

2. Freeze-in production of dark matter from N_1 decay

The singlet fermion S, which is even under the lepton parity, acts as a natural candidate for DM in our scenario. It is known that if a singlet fermion is thermalized, then its freeze-out relic remains overabundant in most of the parameter space. Here, we assume that Snever thermalizes and its relic is realized via the freeze-in mechanism [26–28]. In this case, the freeze-in abundance of S can be obtained from the decay of N_1, σ, H . The DM relic can be obtained from the σ decay after σ is frozen out. However, for the choice of $\lambda_{h\sigma}$ required for FOEWPT, σ will always freeze out with a small relic abundance and hence its contribution to DM is negligible. Another possibility is annihilation of $\sigma\sigma$ to SS with N_1 in the t-channel and u-channel diagrams. However, the rate of these processes are suppressed since the corresponding rate is proportional to y_{NS}^4 . We now discuss the possibility of DM production from N decay. As the reheat temperature, $T_{\rm rh}$, is larger than m_{N_1} , DM can be produced directly from the decay of N_1 . If N_2 is thermally produced, then its decay also contributes to the relic of S. Here, for simplicity, we only consider the decay of N_1 to DM, assuming that the $\overline{N_2}S\sigma$ coupling is negligible. Similarly, the SM Higgs decay to SS at one loop also contributes to the DM relic abundance. However, we note that its contribution is negligible compared to N_1 decay as its rate is proportional to y_{NS}^4 . Nevertheless, here we write the full Boltzmann equations (BE) for the evolution of N_1, σ , and S as

$$\frac{dY_{N_1}}{dz} = -(D_1 + S_1^t + S_1^s)(Y_{N_1} - Y_{N_1}^{\text{eq}})
- \frac{\langle \Gamma_{N_1 \to \sigma S} \rangle}{z\mathcal{H}(T)} \left(Y_{N_1} - Y_S \frac{Y_{N_1}^{\text{eq}}}{Y_S^{\text{eq}}} \right), \quad (3)$$

$$\frac{dY_S}{dz} = \frac{s(T)}{z\mathcal{H}(T)} \left[\langle \sigma v \rangle_{\sigma\sigma\to SS} \left(Y_{\sigma}^2 - Y_S^2 \frac{(Y_{\sigma}^{\text{eq}})^2}{(Y_S^{\text{eq}})^2} \right) + \frac{\langle \Gamma_{\sigma} \rangle}{s(T)} \left(Y_{\sigma} - Y_S \frac{Y_{\sigma}^{\text{eq}}}{Y_S^{\text{eq}}} \right) + 2 \frac{\langle \Gamma_h \rangle}{s(T)} Y_h^{\text{eq}} + \frac{\langle \Gamma_{N_1 \to \sigma S} \rangle}{s(T)} \left(Y_{N_1} - Y_S \frac{Y_{N_1}^{\text{eq}}}{Y_S^{\text{eq}}} \right) \right], \tag{4}$$

$$\frac{dY_{\sigma}}{dz} = \frac{s(T)}{z\mathcal{H}(T)} \left[-\langle \sigma v \rangle_{\sigma\sigma\to SMSM} \left(Y_{\sigma}^{2} - (Y_{\sigma}^{eq})^{2} \right) - \langle \sigma v \rangle_{\sigma\sigma\to SS} \left(Y_{\sigma}^{2} - Y_{S}^{2} \frac{(Y_{\sigma}^{eq})^{2}}{(Y_{S}^{eq})^{2}} \right) - \frac{\langle \Gamma_{\sigma} \rangle}{s(T)} \left(Y_{\sigma} - Y_{S} \frac{Y_{\sigma}^{eq}}{Y_{S}^{eq}} \right) + \frac{\langle \Gamma_{N_{1}\to\sigma S} \rangle}{s(T)} \left(Y_{N_{1}} - Y_{\sigma} \frac{Y_{N_{1}}^{eq}}{Y_{\sigma}^{eq}} \right) \right], \tag{5}$$

where $z=m_{\sigma}/T$, $s(T)=\frac{2\pi^2}{45}g_{*s}T^3$ is the entropy density, $\mathcal{H}(T)=1.66\sqrt{g_*T^2}/M_{\rm pl}$ is the Hubble parameter, $M_{\rm pl}=1.22\times 10^{19}$ GeV is the Planck mass. $\langle \Gamma_{N_1\to\sigma S}\rangle$ is the thermally averaged decay width for $N_1\to\sigma S$, $\langle \Gamma_{\sigma}\rangle$ is the thermally averaged decay width for $\sigma\to S\nu$, $\langle \Gamma_{h}\rangle$ is the thermally averaged decay width for $h\to SS$, $\langle \sigma v\rangle_{\sigma\sigma\to SS}$, $\langle \sigma v\rangle_{\sigma\sigma\to SMSM}$ are the thermally averaged cross-sections involving σ annihilation. $D_1=\langle \Gamma_{N_1\to LH}\rangle/\mathcal{H}z$, where $\langle \Gamma_{N_1\to LH}\rangle$ is the thermally averaged decay width for $N_1\to LH$. $S_i^{s,t}=\Gamma_i^{s,t}/\mathcal{H}z$ are the scattering terms which include both Yukawa and gauge boson contributions involving the visible sector. The expressions for the decay widths and cross sections are given in Appendices C and D.

The N_1LH coupling is related to the neutrino mass and has to be large for larger masses of N_1 . Thus, N_1 will attain equilibrium from the inverse decay $LH \to N_1$. This Yukawa coupling can be computed from the neutrino oscillation data using the Casas-Ibarra (CI) parameterization as given in Eq. A2. We remind that the DM (S) should not be thermalised. Since it has only one annihilation mode, $SS \to \sigma\sigma$ (forbidden channel), DM will freeze out with a larger abundance. This is because the rate of this process is suppressed by the mass of m_{N_1} . To avoid thermalization, y_{NS} is bounded from above. Assuming that the decay happens around the mass scale of N_1 we get

$$y_{NS} \lesssim 4.3 \times 10^{-6} \left(\frac{g_*^d}{100}\right)^{1/4} \left(\frac{m_{N_1}}{10^6 \text{ GeV}}\right)^{1/2},$$
 (6)

where g_*^d is the relativistic degrees of freedom at the time of N_1 decay.

The observed relic of DM can be parameterised in terms of comoving number density Y_S and its mass m_S as

$$\Omega_{\rm DM}h^2 \simeq 0.118 \left(\frac{Y_S}{4.2 \times 10^{-10}}\right) \left(\frac{m_S}{1 \text{ GeV}}\right).$$
(7)

We first solve the BEs 3, 4, 5 simultaneously, fixing $m_{N_1}=10^4~{\rm GeV}, \delta M=2.1\times 10^{-4}~{\rm GeV}, \gamma=0.15-i0.15^2,$ $m_{\sigma}=729.1~{\rm GeV}, \ \lambda_{h\sigma}=6.63,\ m_S=100~{\rm GeV},\ {\rm and}\ y_{NS}=1.56\times 10^{-11}.$ For this choice of $\lambda_{h\sigma}, \sigma$ decouples around $z\sim37$ and freezes out with a yield of $Y_{\sigma}\sim1.3\times 10^{-15}.$ The DM (S) gets produced dominantly from the decay of N_1 and is shown with the blue solid line in Fig. 3. The decay of σ to S after it freezes out does not contribute significantly to the abundance of S. In this scenario the fraction of σ to DM relic is $f_{\sigma}=\Omega_{\sigma}/\Omega_{\rm DM}\sim1.97\times 10^{-3}.$

In Figure 4, we show the correct DM relic contours in the plane y_{NS} vs m_S for the two choices of RHN mass as

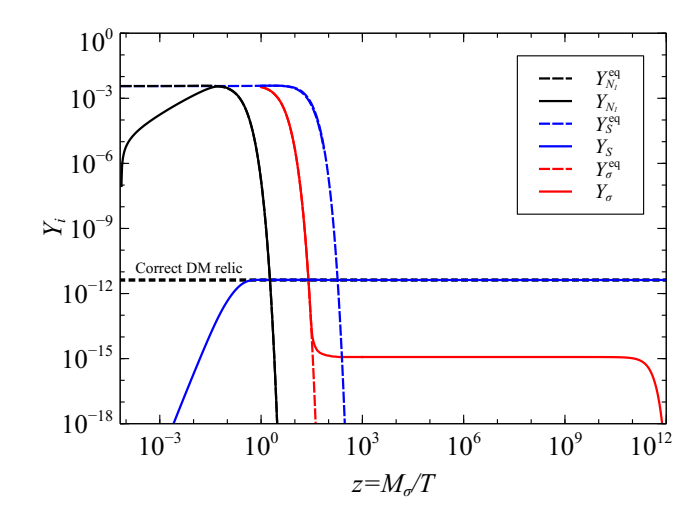


FIG. 3. Cosmological evolution of the abundances of N_1, σ , and S. The corresponding equilibrium abundances are shown with the dashed line. The parameters are fixed at $\{m_{N_1} = 10^4 \text{ GeV}, m_{\sigma} = 729.1 \text{ GeV}, \lambda_{h\sigma} = 6.63, m_S = 100 \text{ GeV}, y_{NS} = 1.56 \times 10^{-11}, \delta M = 2.1 \times 10^{-4} \text{ GeV}, \gamma = 0.15 - i0.15\}.$

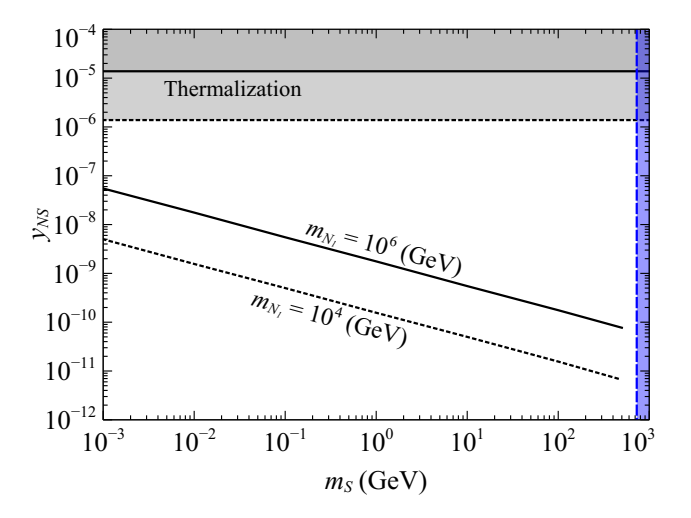


FIG. 4. Correct DM relic contours in the plane of y_{NS} vs m_S for fixed $m_{N_1}=10^6$ GeV (black solid) and $m_{N_1}=10^4$ GeV (black dashed). The correct lepton asymmetry is generated for $\delta M=0.521$ GeV for $m_{N_1}=10^6$ GeV and $\delta M=2.1\times 10^{-4}$ GeV for $m_{N_1}=10^4$ GeV. The rotation angle is fixed at $\gamma=0.15-i0.15$. The region of thermalization of DM is shown with gray shading for these two masses, respectively. The blue shaded region corresponds to $m_S>m_\sigma$.

 $m_{N_1}=10^4$ and 10^6 GeV. The correct lepton asymmetry can be obtained for these two masses by fixing the mass splitting $\delta M=2.1\times 10^{-4}$ GeV and 0.521 GeV respectively, where γ is fixed at 0.15 – i0.15. In the upper gray shaded region, the DM will come to thermal equilibrium; hence, it is disallowed in our scenario. The blue shaded region corresponds to $m_S>m_\sigma$.

As already discussed, large values of $\lambda_{h\sigma}$ will lead to FOEWPT, which results in stochastic GWs. In Fig. 5, we show the GW spectrum corresponding to the same

² Here γ is the complex rotation angle used in the CI parameterization, and $\delta M = m_{N_2} - m_{N_1}$, where m_{N_i} is the mass of N_i .

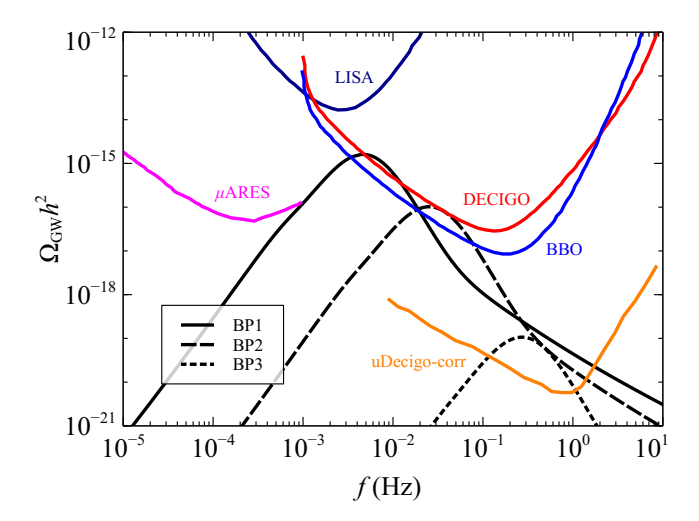


FIG. 5. Gravitational wave spectrum from first order electroweak phase transition for BP1, BP2, and BP3 as mentioned in Fig. 2.

benchmark point as in Fig. 3, which we call BP1. This is shown as a cyan star in Fig. 2. We also show the spectrum for another two choices of $\{\lambda_{h\sigma}, m_{\sigma}\}$, as shown with yellow and red stars in Fig. 2. The details of the BPs are given in Table I. The peak lies within the projected sensitivities of the BBO and DECIGO experiments, while the low and high frequency tails extend into the sensitivity ranges of μ ARES and uDECIGO-corr, respectively.

B. Consequences of Small $\lambda_{h\sigma}$

1. Freeze-in and SuperWIMP production of DM

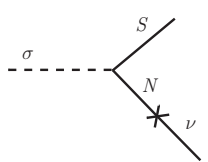


FIG. 6. Feynman diagram of σ decay to S and ν .

If $\lambda_{h\sigma}$ coupling is small compared to the previous case, σ freezes out with a relatively larger abundance. In this case, the late decay of $\sigma \to S\nu$, as shown in Fig. 6, can also produce some amount of DM, which is known as the SuperWIMP contribution, $\Omega_{\text{SuperWIMP}}h^2$. The component of DM generated from N_1 decay is known as the freeze-in component, $\Omega_{\text{f.i.}}h^2$. Thus, the total DM relic abundance is found to be

$$\Omega_{\rm DM}h^2 = \Omega_{\rm f.i.}h^2 + \Omega_{\rm SuperWIMP}h^2.$$
(8)

Now the late decay of σ not only contributes to DM but also enhances the number of relativistic d.o.f. by injecting additional ν_L from the same decay mode. This

happens if the decay occurs after the SM neutrino decoupling, which we assume to be $T_{\nu}^{\rm dec} \sim 1$ MeV and before the CMB epoch: $T_{\rm CMB} \sim 0.26$ eV.

2. $\Delta N_{\rm eff}$ from late decay of σ

If the decay $\sigma \to S\nu$ happens after the SM neutrinos decouple from the thermal bath, then it can give rise to additional light d.o.f. In the absence of these light d.o.f., the SM gives a precise prediction for $N_{\rm eff}$, namely $N_{\rm eff}^{\rm SM} = 3.045$ [29–31]. The additional contribution to the effective number of relativistic species at the CMB epoch from σ decay is given as

$$\Delta N_{\text{eff}} = N_{\text{eff}} - N_{\text{eff}}^{\text{SM}} = N_{\nu} \frac{\rho_{\nu_L}}{\rho_{\nu_L}^{\text{SM}}} \bigg|_{T_{\text{CMB}}}, \tag{9}$$

where $N_{\nu}=3$ is the number of generations of SM neutrinos, $\rho_{\nu_L}^{\rm SM}=2\frac{7}{8}\frac{\pi^2}{30}T_{\nu_L}^4$ is the energy density of the SM neutrino, ρ_{ν_L} is the late time produced neutrino energy density. The DESI 2024 [10] data put an upper bound on $\Delta N_{\rm eff}$ as 0.39. Planck 2018 [11] put a constraint as $\Delta N_{\rm eff}<0.285$. The ACT 2025 [12] data constrain $\Delta N_{\rm eff}$ to be $\Delta N_{\rm eff}<0.32$. The combined Planck and ACT [12] data further tighten this constraint to be $\Delta N_{\rm eff}<0.14$. The future CMB experiment SPT-3G [13] is expected to be sensitive down to $\Delta N_{\rm eff}=0.1$. The CMB-S4 [14] can probe down to 0.06, whereas CMB-HD [15] can probe $\Delta N_{\rm eff}$ down to 0.027.

The evolution of the energy density of these late-time produced neutrinos is governed by the following BE

$$\frac{d\rho_{\nu_L}}{dz} = -\frac{4\beta\rho_{\nu_L}}{z} + \frac{1}{z\mathcal{H}(z)} \langle E\Gamma_{\sigma} \rangle Y_{\sigma} s(z), \tag{10}$$

where

$$\beta = 1 + \frac{T}{3g_s(T)} \frac{dg_s}{dT}.$$
 (11)

Here g_s is the effective number of d.o.f. contributing to the entropy density. The thermally averaged energy transfer rate is given as [32, 33]

$$\langle E\Gamma_{\sigma}\rangle = g_S g_{\nu} \frac{|\mathcal{M}|_{\sigma \to S\nu}^2}{32\pi} \frac{(m_{\sigma}^2 - m_S^2)^2}{m_{\sigma}^4}, \tag{12}$$

where the matrix-squared element for this decay process is given as

$$|\mathcal{M}|_{\sigma \to S\nu}^2 = \frac{y_{NS}^2 y^2 v_h^2}{2m_{N_1}^2} (m_\sigma^2 - m_S^2)$$
 (13)

Now to obtain the energy density of these additional neutrinos, we need to solve Eq. 10, together with Eqs. 3, 4, 5. We fix the parameters as $m_{N_1}=10^4$ GeV, $\delta M=2.1\times 10^{-4}$ GeV, $\gamma=0.15-i0.15,\ m_S=100$ GeV, $y_{NS}=1.5\times 10^{-11},\ m_\sigma=500$ GeV, and $\lambda_{h\sigma}=0.3$.

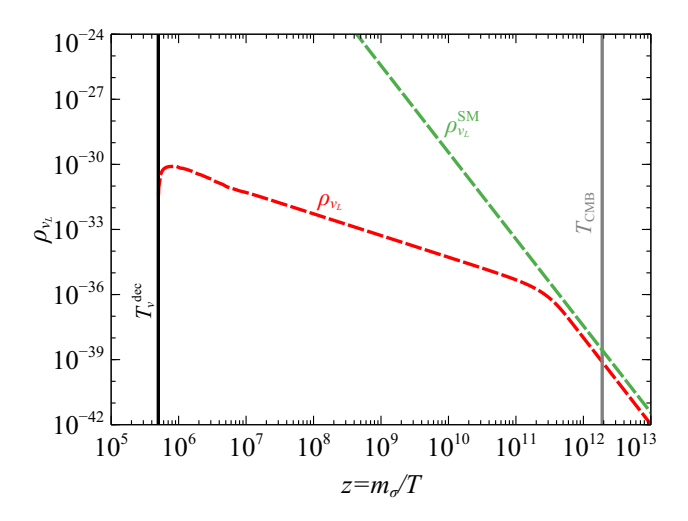


FIG. 7. The cosmological evolution of the energy density of the neutrino from σ decay (red dashed line) and the SM neutrino (green dashed line) is shown as a function of $z (= m_{\sigma}/T)$.

In this case, σ contribution to DM relic is found to be $f_{\sigma} \times 0.12 \times \frac{m_S}{m_{\sigma}} = 6.48 \times 10^{-3}$, where $f_{\sigma} = 0.27$. For this choice of parameters, we found that the contribution of σ to DM relic density is around $\sim 5\%$. However, its contribution to the $\Delta N_{\rm eff}$ is calculated to be 0.858, which is much larger than the current constraints from CMB experiments. In Fig. 7, we show the evolution of the energy density of ν_L originating from σ decay, with a red dashed line. The cosmological evolution of SM neutrino energy density is shown with the green dashed line. The neutrino decoupling and the CMB temperatures are shown with the black and gray solid vertical lines, respectively.

We now obtain the correct DM relic contours in the plane of y_{NS} vs $\lambda_{h\sigma}$ for fixed $m_{\sigma} = 500$ GeV, $m_{N_1} = 10^4$ GeV, $\delta M = 2.1 \times 10^{-4}$ GeV, and $\gamma = 0.15 - i0.15$ and shown in the left panel of Fig. 8. We take two values of DM mass, $m_S = 1$ GeV (black line) and $m_S = 100$ GeV (gray line). DM relic is obtained considering both the freeze-in $(N_1 \text{ decay})$ and SuperWIMP $(\sigma \text{ decay})$ contributions. The color code represents the percentage of freeze-in component to the total DM relic. As the $\lambda_{h\sigma}$ coupling decreases, the freeze-out abundance of σ increases. This leads to an increment in the SuperWIMP component of the DM relic. Now, for the correct relic of DM, the freeze-in part needs to decrease, which implies further smaller values of y_{NS} . This behavior can be clearly read from the *left* panel of Fig. 8. As the $\lambda_{h\sigma}$ coupling is increased, the freeze-out abundance of σ gets reduced, leading to a smaller SuperWIMP contribution. With very large $\lambda_{h\sigma}$, the freeze-in component becomes almost 100% (dark blue points), and the relic becomes independent of y_{NS} for a fixed DM mass. For a smaller DM mass, the contour shifts upward. This is because the relic, $\Omega_{\rm DM}h^2 \propto m_S Y_S$, as m_S decreases, Y_S has to increase, to fix $\Omega_{\rm DM}h^2$. An increment in y_{NS} will lead to an increment in Y_S .

For these same points given in *left* panel of Fig. 8, we calculate the $\Delta N_{\rm eff}$ and show as a function of $\lambda_{h\sigma}$ in the right panel of Fig. 8. For smaller $\lambda_{h\sigma}$, σ decouples with larger abundance. As a result, the correct relic abundance can be obtained from the SuperWIMP component (σ decay), leading to a negligible freeze-in component which requires a relatively smaller y_{NS} coupling. When the Yukawa coupling, y_{NS} , is small, σ decays at a late epoch with a larger $\Delta N_{\rm eff}$ as the σ abundance is large. On the other hand, an increase of $\lambda_{h\sigma}$ will lead to a decrease in σ abundance, leading to a smaller $\Delta N_{\rm eff}$ through σ decay. This is clearly visible in the right panel of Fig. 8. To summarize, a red point implies zero freezein component and large $\Delta N_{\rm eff}$. Similarly, the blue point represents 100% freeze-in component with small $\Delta N_{\rm eff}$. The Planck data exclude $\lambda_{h\sigma} \lesssim 0.16 \ (0.55)$ for 1 GeV (100 GeV) DM mass. In this parameter space, the contribution of the SuperWIMP component to the DM relic remains $\lesssim 3\%$. The future CMB-HD experiment will be able to exclude $\lambda_{h\sigma} \lesssim 0.55$ (2) for 1 GeV (100 GeV) DM

We then fix $m_S = 1$ GeV, $m_{N_1} = 10^4$ GeV, $\delta M =$ 2.1×10^{-4} GeV, and $\gamma = 0.15 - i0.15$ and calculate the DM relic for two choices of m_{σ} as 100 GeV (black solid line) and 1000 GeV (gray solid line) and shown in Fig. 9 in the $y_{NS} - \lambda_{h\sigma}$ plane. The color-code represents the percentage of freeze-in component to the total DM relic, similar to Fig. 8. As the $\lambda_{h\sigma}$ coupling decreases, the freeze-out abundance of σ increases, thereby enhancing the SuperWIMP contribution to the DM relic. To obtain the correct relic abundance, the freeze-in component must accordingly decrease, which requires a reduction in the value of y_{NS} . This behavior is evident in the left panel of Fig. 9. Conversely, as the $\lambda_{h\sigma}$ coupling increases, the freeze-out abundance of σ decreases, leading to a reduced SuperWIMP contribution to the total relic density. For sufficiently large $\lambda_{h\sigma}$, the freeze-in contribution dominates almost entirely (blue points), and the relic abundance becomes independent of y_{NS} for a fixed DM mass. For the same points, we now compute $\Delta N_{\rm eff}$ and present it as a function of $\lambda_{h\sigma}$ in the *right* panel of Fig. 9. Here, the Planck data exclude $\lambda_{h\sigma} \lesssim 0.055$ (0.26) for 100 GeV (1000 GeV) σ mass. In this parameter space, the contribution of the SuperWIMP component to the DM relic remains $\lesssim 1\%$. The future CMB-HD experiment will be able to exclude $\lambda_{h\sigma} \lesssim 0.19 \ (0.95)$ for 100 GeV (1000 GeV) σ mass.

Based on the above discussion, we conclude that the current constraints on $\Delta N_{\rm eff}$ restrict the SuperWIMP contribution (σ decay) to be $\lesssim 3\%$ to the total DM relic. Therefore, for $T_{\rm rh} > m_{N_1}$, the DM relic is solely decided by the freeze-in component (N_1 decay).

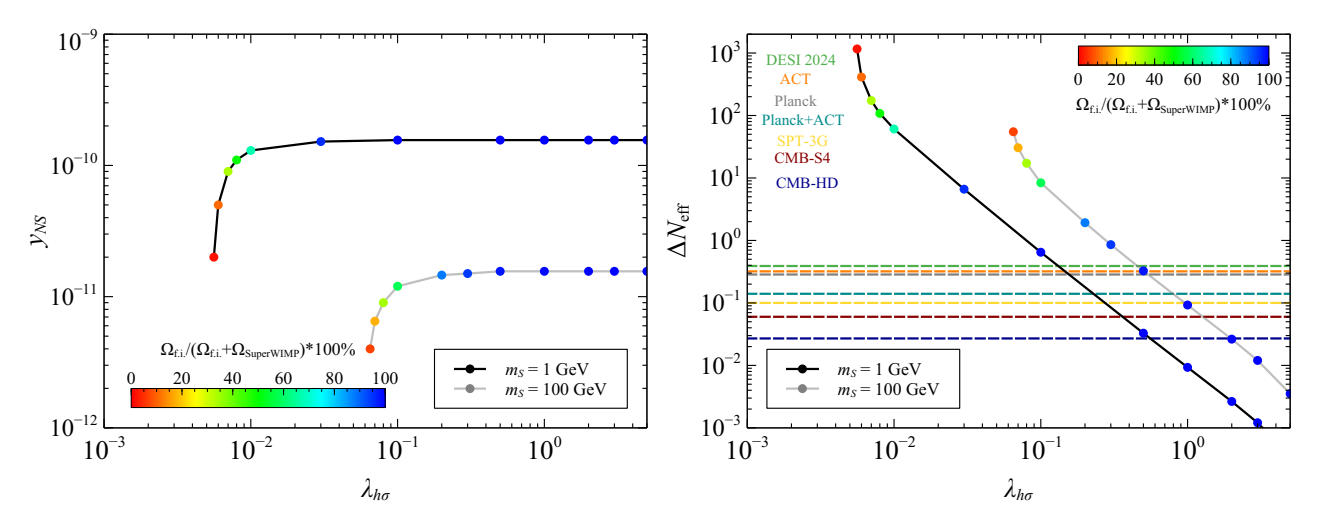


FIG. 8. [Left:] Correct relic contours in the $y_{NS} - \lambda_{h\sigma}$ plane for two DM masses: $m_S = 1$ GeV (black solid line) and $m_S = 100$ GeV (gray solid line). The other parameters are fixed as $\{m_{\sigma} = 500$ GeV, $m_{N_1} = 10^4$ GeV, $\delta M = 2.1 \times 10^{-4}$ GeV, $\gamma = 0.15 - i0.15\}$. The color code denotes the fraction of freeze-in DM relic from N_1 decay to the total DM relic. [Right:] The same points in the $\Delta N_{\rm eff} - \lambda_{h\sigma}$ plane with same color code.

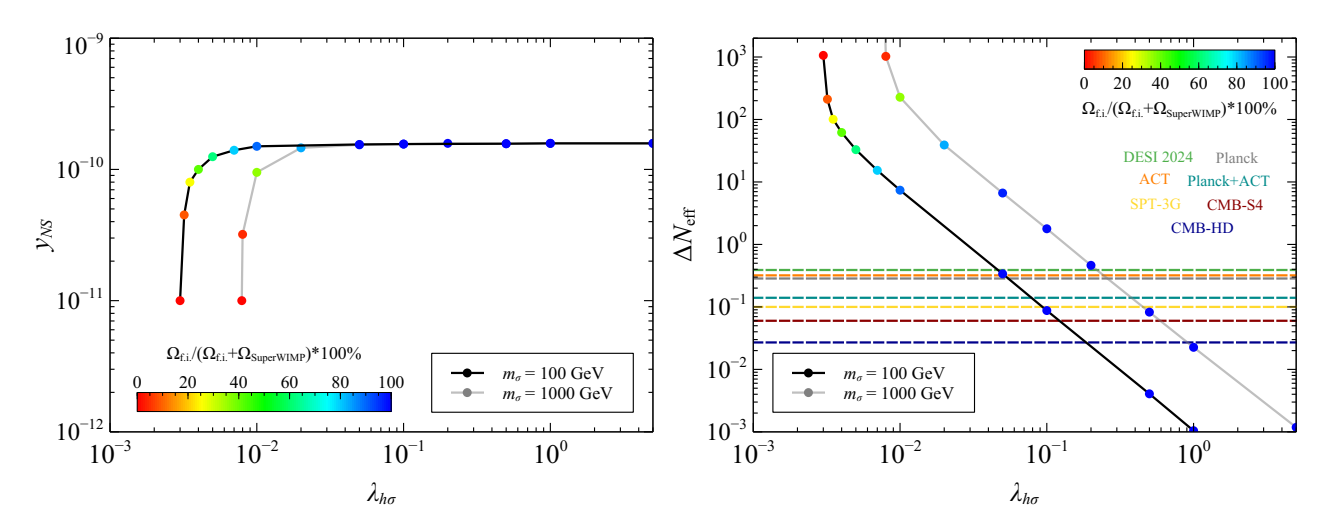


FIG. 9. [Left:] Correct relic contours in the $y_{NS} - \lambda_{h\sigma}$ plane for two σ masses: $m_{\sigma} = 100$ GeV (black solid line) and $m_{\sigma} = 1000$ GeV (gray solid line). The other parameters are fixed as $\{m_S = 1 \text{ GeV}, m_{N_1} = 10^4 \text{ GeV}, \delta M = 2.1 \times 10^{-4} \text{ GeV}, \gamma = 0.15 - i0.15\}$. The color code denotes the fraction of freeze-in relic to the total DM relic. [Right:] The same points in the $\Delta N_{\text{eff}} - \lambda_{h\sigma}$ plane.

IV. PHENOMENOLOGY WITH $T_{\rm EW} < T_{\rm rh} \ll m_{N_1}$: DM PRODUCTION FROM h DECAY

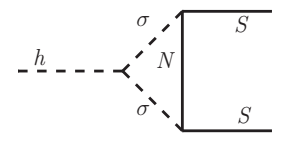


FIG. 10. Feynman diagram for DM production from h decay.

We now turn to the possibility of a low reheating scenario with $T_{\rm EW} < T_{\rm rh} \ll m_{N_1}$. The detectability of the scenario, at future GW experiments and CMB experiments, remains the same as discussed in section III. If

 $T_{\rm rh} > m_{\sigma}$, then σ particles are also produced abundantly. As concluded in the previous section, σ does not play any role in the DM relic. Therefore, in this scenario, the DM relic abundance is determined solely by the one–loop decay of the Higgs, $h \to SS$ as shown in Fig. 10. This restricts the DM mass to $m_S < m_h/2$. The effective vertex can be written as $y_{\rm eff}hSS$, where the effective coupling is given in Appendix C. In this scenario, the Boltzmann equation reduces to

$$\frac{dY_S}{dz} = 2 \frac{\langle \Gamma_h \rangle}{z \mathcal{H}(T)} Y_h^{\text{eq}}, \tag{14}$$

where $\langle \Gamma_h \rangle$ is the thermally averaged decay width of Higgs to SS given in Appendix C. We find the correct DM relic contour in the plane of y_{eff} vs m_S and show it

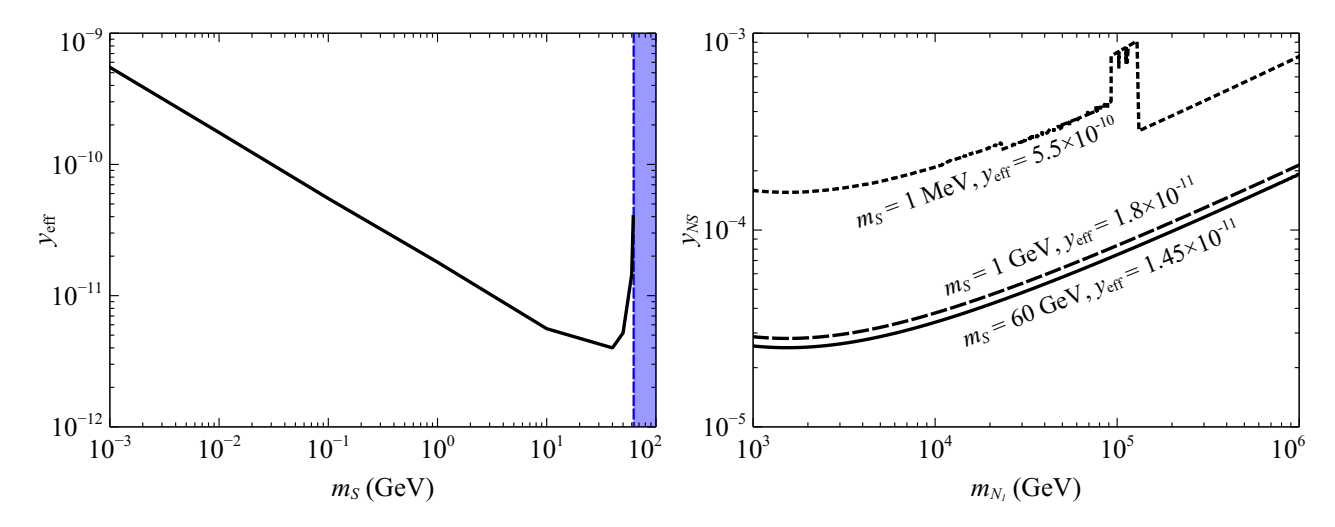


FIG. 11. [Left:] correct relic contour in the plane $y_{\rm eff}-m_S$. In the blue shaded region, $m_S>m_h/2$. [Right:] correct relic contour in the plane $y_{NS}-m_{N_1}$ for $m_S=1$ MeV (dotted), $m_S=1$ GeV (dashed), $m_S=60$ GeV (solid), $m_\sigma=729.1$ GeV, $\lambda_{h\sigma}=6.63$.

with the black solid line in the left panel of Fig. 11. The blue shaded region is excluded since $m_S > m_h/2$ in that region. From the left panel of Fig. 11 we see that as the DM mass increases, the $y_{\rm eff}$ coupling decreases to give the correct DM relic. When the DM mass approaches $m_h/2$, the decay width decreases, and hence the abundance. Now, to get the correct relic of DM, $y_{\rm eff}$ has to increase. This behavior is clearly visible in the left panel of Fig. 11. $y_{\rm eff}$ is a function of $\{y_{NS}, m_{N_1}, m_{\sigma}, \lambda_{h\sigma}, m_S\}$. We then take three sets of $\{m_S, y_{\rm eff}\}$ values from the left panel of Fig. 11 and show the allowed values of y_{NS} and m_{N_1} by fixing $m_{\sigma} = 729.1$ GeV and $\lambda_{h\sigma} = 6.63$. This choice of parameters leads to FOEWPT, as shown with a cyan star in Fig. 2.

V. CONCLUSION

In this study, we have explored the realization of freezein dark matter within a minimal extension of the type-I seesaw framework, where the remnant lepton-parity symmetry naturally plays the role of a dark parity. By introducing a lepton parity even singlet fermion S and a lepton parity odd scalar σ , the setup naturally accommodates a stable dark matter candidate. The CPviolating, out-of-equilibrium decays of nearly degenerate right-handed neutrinos (N) generate a lepton asymmetry via flavored resonant leptogenesis, which is subsequently converted into the observed baryon asymmetry through electroweak sphaleron processes. The fermion S acts as a natural freeze-in dark matter candidate, with its production determined by the thermal history of the early Universe. For reheating temperatures, $T_{\rm rh} > m_{N_1}$, the dominant contribution to the DM relic density originates from right-handed neutrino decays, while for $T_{\rm EW} < T_{\rm rh} \ll$ m_{N_1} , it can be produced via Higgs decay. Direct and indirect detection constraints on DM are naturally avoided

due to the extremely small Yukawa couplings. However, this scenario can leave observable imprints through gravitational waves and at CMB experiments. When the $h-\sigma$ coupling is larger (typically $\lambda_{h\sigma}>1$), then the EWPT can be first-order and gives rise to stochastic gravitational waves which can be detected at different GW experiments like DECIGO, BBO, etc. On the other hand if $h-\sigma$ coupling is small (typically $\lambda_{h\sigma}\ll 1$), then the late decay of σ can give rise observable $\Delta N_{\rm eff}$. In conclusion, our model provides a scenario connecting dark matter production, leptogenesis, $\Delta N_{\rm eff}$, and electroweak symmetry breaking dynamics in a unified and testable framework.

ACKNOWLEDGMENTS

P.K.P. acknowledges the Ministry of Education, Government of India, for providing financial support for his research via the Prime Minister's Research Fellowship (PMRF) scheme. P.K.P. would like to thank Santu Kumar Manna for his assistance with CosmoTransitions.

Appendix A: Flavored-resonant leptogenesis

In this minimal scenario of type-I seesaw with two RHNs, two non-zero light neutrino masses can be obtained and are given by

$$m_{\nu} = \frac{v_h^2}{2} y M^{-1} y^T. \tag{A1}$$

Here, the 3×2 Yukawa coupling matrix can be parameterized as

$$y = \frac{\sqrt{2}}{v_b} U_{\text{PMNS}} \sqrt{\hat{m}_{\nu}} \mathcal{R}^T . \sqrt{\hat{M}}, \tag{A2}$$

where $U_{\rm PMNS}$ is the Pontecorvo–Maki–Nakagawa–Sakata matrix, $\hat{m}_{\nu} = {\rm diag}(0,m_2,m_3)$ is the diagonal light neutrino mass matrix, $\hat{M} = {\rm diag}(m_{N_1},m_{N_2})$ is the diagonal heavy RHN matrix and \mathcal{R} is the orthogonal rotational matrix defined as

$$\mathcal{R} = \begin{pmatrix} 0 & \cos \gamma & \sin \gamma \\ 0 & -\sin \gamma & \cos \gamma \end{pmatrix},\tag{A3}$$

where γ is the complex rotation angle.

A very high-scale seesaw places the viability of the leptogenesis scenario beyond the reach of current experimental facilities. However, the leptogenesis scale can be lowered by considering resonant enhancement of the CP asymmetry [34]. The impact of lepton flavor in leptogenesis becomes significant once the charged lepton interactions with the thermal bath reach equilibrium. At very high temperatures, these interactions are negligible, and all lepton flavors remain coherent. As the Universe cools, the Yukawa interactions of the charged leptons successively enter equilibrium [35]. Around $T \sim 10^{12}$ GeV, the τ Yukawa coupling is strong enough to thermalize the τ flavor. By $T \sim 10^9$ GeV, the μ Yukawa interaction also equilibrates. Below this scale, all three lepton flavors are effectively distinguished. In standard resonant leptogenesis, a mild mass degeneracy between the RHNs N_1, N_2 results in a resonant enhancement of the CP asymmetry via contributions from the self-energy diagrams. The CP violating out-of-equilibrium decay of N_1 , and N_2 to L_{α} , H generates the lepton asymmetry in the early Universe in different flavors. The key parameters in the leptogenesis are $\{m_{N_1}, \delta M, \gamma\}$, where $\delta M = m_{N_2} - m_{N_1}$ and γ is the complex rotation angle of the orthogonal matrix used in the Casas-Ibarra (CI) parametrization in Appendix A. In the flavored regime, the evolution of the lepton asymmetry is governed by the density matrix formalism, with the diagonal elements representing flavor-specific asymmetries and the off-diagonal elements encoding quantum coherence between flavors. For TeV-scale leptogenesis, rapid thermal interactions erase this coherence, strongly damping the off-diagonal terms. Consequently, the density matrix equations simplify to a set of flavor-diagonal Boltzmann equations, one for each lepton flavor asymmetry. This simplification remains valid when $m_{N_i} \ll 10^9 \text{ GeV}$ [36, 37]. In our analysis, we have incorporated all relevant lepton-number-violating processes, including both Yukawa-mediated and gauge-mediated channels. gauge processes, in particular, are crucial, as their typically strong interaction rates keep them in equilibrium over a wide temperature range, leading to a significant enhancement of washout effects. The produced lepton asymmetry is subsequently converted into baryon asymmetry via electroweak sphalerons. This process must be completed before $T_{\rm sph} > 131.7 \; {\rm GeV} \; [38].$

The CP asymmetry parameter for the decay of N_i into

 L_{α} is given as [39, 40]

$$\epsilon_{\alpha\alpha}^{i} = -\sum_{j\neq i} \frac{\operatorname{Im}\left[(y^{\dagger})_{i\alpha}(y)_{\alpha j}(y^{\dagger}y)_{ij} + \frac{m_{N_{i}}}{m_{N_{j}}}(y^{\dagger})_{i\alpha}y_{\alpha j}(y^{\dagger}y)_{ji} \right]}{(y^{\dagger}y)_{ii}(y^{\dagger}y)_{jj}} \times \left(\frac{(m_{N_{i}}^{2} - m_{N_{j}}^{2})m_{N_{i}}\Gamma_{j}}{(m_{N_{i}}^{2} - m_{N_{j}}^{2})^{2} + m_{N_{i}}^{2}\Gamma_{j}^{2}} + \frac{(m_{N_{i}}^{2} - m_{N_{j}}^{2})m_{N_{i}}\Gamma_{j}}{(m_{N_{i}}^{2} - m_{N_{j}}^{2})^{2} + (m_{N_{i}}\Gamma_{i} + m_{N_{j}}\Gamma_{j})^{2} \frac{\det[\operatorname{Re}(y^{\dagger}y)]}{(y^{\dagger}y)_{ii}(y^{\dagger}y)_{jj}} \right)}$$
(A4)

The Boltzmann equations driving the abundance of N_2 , and asymmetries in different flavors are given as

$$\frac{dY_{N_2}}{dz} = -(D_2 + S_2^t + S_2^s)(Y_{N_2} - Y_{N_2}^{\text{eq}}), \quad (A5)$$

$$\frac{dY_{\Delta e}}{dz} = \epsilon_{ee}^{1} D_{1} (Y_{N_{1}} - Y_{N_{1}}^{\text{eq}}) + \epsilon_{ee}^{2} D_{2} (Y_{N_{2}} - Y_{N_{2}}^{\text{eq}})
- \left(W_{1}^{D} + W_{1}^{t} + \frac{Y_{N_{1}}}{Y_{N_{1}}^{\text{eq}}} W_{1}^{s} \right) \left(\frac{|y_{e1}|^{2}}{(y^{\dagger}y)_{11}} \right) Y_{\Delta e}
- \left(W_{2}^{D} + W_{2}^{t} + \frac{Y_{N_{2}}}{Y_{N_{2}}^{\text{eq}}} W_{2}^{s} \right) \left(\frac{|y_{e2}|^{2}}{(y^{\dagger}y)_{22}} \right) Y_{\Delta e}
- W_{\Delta L2} Y_{\Delta e},$$
(A6)

$$\frac{dY_{\Delta\mu}}{dz} = \epsilon_{\mu\mu}^{1} D_{1} (Y_{N_{1}} - Y_{N_{1}}^{\text{eq}}) + \epsilon_{\mu\mu}^{2} D_{2} (Y_{N_{2}} - Y_{N_{2}}^{\text{eq}})
- \left(W_{1}^{D} + W_{1}^{t} + \frac{Y_{N_{1}}}{Y_{N_{1}}^{\text{eq}}} W_{1}^{s} \right) \left(\frac{|y_{\mu 1}|^{2}}{(y^{\dagger}y)_{11}} \right) Y_{\Delta\mu}
- \left(W_{2}^{D} + W_{2}^{t} + \frac{Y_{N_{2}}}{Y_{N_{2}}^{\text{eq}}} W_{2}^{s} \right) \left(\frac{|y_{\mu 2}|^{2}}{(y^{\dagger}y)_{22}} \right) Y_{\Delta\mu},
- W_{\Delta L2} Y_{\Delta\mu},$$
(A7)

$$\frac{dY_{\Delta\tau}}{dz} = \epsilon_{\tau\tau}^{1} D_{1} (Y_{N_{1}} - Y_{N_{1}}^{\text{eq}}) + \epsilon_{\tau\tau}^{2} D_{2} (Y_{N_{2}} - Y_{N_{2}}^{\text{eq}})
- \left(W_{1}^{D} + W_{1}^{t} + \frac{Y_{N_{1}}}{Y_{N_{1}}^{\text{eq}}} W_{1}^{s} \right) \left(\frac{|y_{\tau 1}|^{2}}{(y^{\dagger}y)_{11}} \right) Y_{\Delta\tau}
- \left(W_{2}^{D} + W_{2}^{t} + \frac{Y_{N_{2}}}{Y_{N_{2}}^{\text{eq}}} W_{2}^{s} \right) \left(\frac{|y_{\tau 2}|^{2}}{(y^{\dagger}y)_{22}} \right) Y_{\Delta\tau},
- W_{\Delta L2} Y_{\Delta\tau},$$
(A8)

The abundance, Y_i is defined as $Y_i = n_i/s$. $D_i = \langle \Gamma_{N_i \to LH} \rangle / \mathcal{H}z$, where $\langle \Gamma_{N_i \to LH} \rangle$ is the thermally averaged decay width for $N_i \to LH$. $S_i^{s,t} = \Gamma_i^{s,t} / \mathcal{H}z$ are the scattering terms which include both Yukawa and gauge boson contributions, W_i^D corresponds to the washout term due to inverse decay, $W_i^{s,t}$ represent the washout due to $\Delta L = 1$ scatterings considering both Yukawa coupling driven processes and gauge boson involved processes and $W_{\Delta L2}$ represents the $\Delta L = 2$ washout. We follow the notations of [41].

The baryon asymmetry then can be written in terms of the lepton asymmetries as

$$\eta_B = 7.04 \frac{C}{f} (Y_{\Delta e} + Y_{\Delta \mu} + Y_{\Delta \tau}) = 7.04 \frac{C}{f} Y_{\Delta}, \quad (A9)$$

where C=28/79 is the fraction of lepton asymmetry converted into a baryon asymmetry by sphaleron processes, $f=g_s^*/g_0^*=28^3$ is the dilution factor calculated assuming standard photon production from the onset of leptogenesis till recombination, and N_{Δ} denotes the total lepton asymmetry.

In Fig. 12, we show the evolution of the asymmetries as well as the abundances of RHNs and DM. The parameters are fixed at the same value as in Fig. 3. The

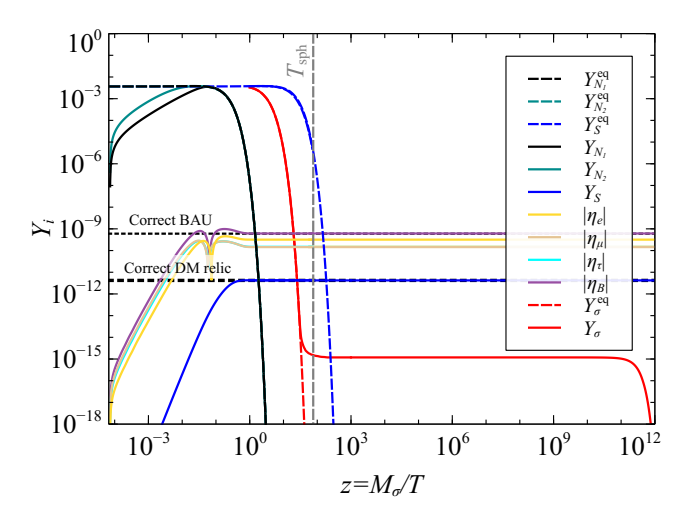


FIG. 12. Cosmological evolution of the abundances of N_1, N_2, σ , S, and lepton asymmetries. The corresponding equilibrium abundances are shown with the dashed line. The parameters are fixed at $\{m_{N_1} = 10^4 \text{ GeV}, m_{\sigma} = 729.1 \text{ GeV}, \lambda_{h\sigma} = 6.63, m_S = 100 \text{ GeV}, y_{NS} = 1.56 \times 10^{-11}, \delta M = 2.1 \times 10^{-4} \text{ GeV}, \gamma = 0.15 - i0.15$. Here $\eta_i = 7.04 \frac{C}{f} Y_{\Delta i}$. The vertical gray dashed line represents the sphaleron transition temperature.

vertical gray dashed line represents the sphaleron transition temperature. The observed baryon asymmetry and DM relic values are indicated with black dashed lines.

Appendix B: Finite-Temperature Effective Potential

The finite temperature effective potential can be written as

$$V_{\text{eff}} = V_0(h) + V_{\text{cw}}(h) + V_{\text{ct}}(h) + V_T(h, T) + V_{\text{daisy}}(h, T),$$
 (B1)

where the tree-level potential is given as

$$V_0(h) = -\frac{\mu_h^2}{2}h^2 + \frac{\lambda_h}{4}h^4.$$
 (B2)

The one-loop Coleman-Weinberg zero temperature contribution in $\overline{\rm MS}$ renormalization scheme is given as

$$V_{\text{cw}}(h) = \sum_{i} (-1)^{F_i} \frac{n_i^2}{64\pi^2} m_i^2(h) \left(\log \left(\frac{m_i^2(h)}{m_i^2(v_h)} \right) - c_i \right),$$
(B3)

where F_i denotes fermion number, which is 1 for fermions and 0 for bosons, $c_i = 3/2$ for fermions and scalars, and $c_i = 5/6$ for vector bosons, $m_i(h)$ are the fields dependent masses given as

$$m_h^2(h) = -\mu_h^2 + 3\lambda_h h^2, \ n_h = 1,$$

$$m_{GB}^2(h) = -\mu_h^2 + \lambda_h h^2, \ n_{GB} = 1,$$

$$m_{\sigma}^2(h) = \mu_{\sigma}^2 + \lambda_{h\sigma} h^2, \ n_{\sigma} = 1,$$

$$m_t^2(h) = \frac{y_t^2}{2} h^2, \ n_t = 12,$$

$$m_W^2(h) = \frac{g^2}{4} h^2, \ n_W = 6,$$

$$m_Z^2(h) = \frac{g^2 + g'^2}{4} h^2, \ n_Z = 3.$$
 (B4)

The counter term is

$$V_{\rm ct}(h) = -\frac{\delta\mu_h^2}{2}h^2 + \frac{\delta\lambda_h}{4}h^4,\tag{B5}$$

which is derived by solving

$$\frac{\partial (V_{\text{cw}} + V_{\text{ct}})}{\partial h}|_{h=v_h} = 0, \frac{\partial^2 (V_{\text{cw}} + V_{\text{ct}})}{\partial h^2}|_{h=v_h} = 0.$$
 (B6)

The finite temperature contribution to the effective potential is given as

$$V_T(h,T) = \frac{T^4}{2\pi^2} \left[\sum_{i \in B} n_i J_B \left(\frac{m_i(h)}{T} \right) - \sum_{j \in F} n_j J_F \left(\frac{m_j(h)}{T} \right) \right],$$
(B7)

where

$$J_{B/F}(y) = \int_0^\infty x^2 \log(1 \mp e^{-\sqrt{x^2 + y^2}})$$
 (B8)

The daisy contribution is

$$V_{\text{daisy}}(h,T) = \sum_{i} \frac{T}{12\pi} n_i \left[m_i^3(h) - \left(m_i^2(h) + \Pi_i(T) \right)^{3/2} \right],$$
(B9)

 $^{^3}$ $g_s^* = 106.75 + \frac{7}{8} \times 2 + 1 = 109.5$ is the relativistic degrees of freedom (d.o.f) at the onset of leptogenesis in our scenario, $g_0^* = 3.91$ is the present day relativistic d.o.f.

where n_i denotes all d.o.f. for scalars and only longitudinal d.o.f. for vector bosons and Π_i s are given as

$$\Pi_{h}(T) = T^{2} \left(\frac{1}{2}\lambda_{h} + \frac{1}{4}y_{t}^{2} + \frac{3}{16}g^{2} + \frac{1}{16}g'^{2} + \frac{1}{12}\lambda_{h\sigma}\right), \qquad \sqrt{m_{\sigma}^{4} + (m_{N_{1}}^{2} - m_{S}^{2})^{2} - 2m}$$

$$\Pi_{GB}(T) = T^{2} \left(\frac{1}{2}\lambda_{h} + \frac{1}{4}y_{t}^{2} + \frac{3}{16}g^{2} + \frac{1}{16}g'^{2} + \frac{1}{12}\lambda_{h\sigma}\right), \qquad \Gamma_{\sigma \to S\nu} = \frac{m_{\sigma}}{32\pi} \frac{y_{NS}^{2}y^{2}v_{h}^{2}}{m_{N_{1}}^{2}} \left(1 - \frac{m_{N_{1}}^{2}}{m_{N_{2}}^{2}}\right), \qquad \Gamma_{h \to SS} = \frac{1}{2}\left[(g^{2} + g'^{2})(\frac{11}{6}T^{2} - \frac{1}{4}h^{2}) + \frac{1}{4}g^{2}g'^{2}h^{4}\right], \qquad \gamma_{h \to SS} = \frac{1}{2}\left[(g^{2} + g'^{2})(\frac{11}{6}T^{2} + \frac{1}{4}h^{2})^{2} + \frac{1}{4}g^{2}g'^{2}h^{4}\right], \qquad \gamma_{h \to SS} = \frac{1}{2}\left[(g^{2} + g'^{2})(\frac{11}{6}T^{2} + \frac{1}{4}h^{2})^{2} + \frac{1}{4}g^{2}g'^{2}h^{4}\right], \qquad \gamma_{h \to SS} = \frac{1}{2}\left[(g^{2} + g'^{2})(\frac{11}{6}T^{2} + \frac{1}{4}h^{2})^{2} + \frac{1}{4}g^{2}g'^{2}h^{4}\right], \qquad \gamma_{h \to SS} = \frac{1}{2}\left[(g^{2} + g'^{2})(\frac{11}{6}T^{2} + \frac{1}{4}h^{2})^{2} + \frac{1}{4}g^{2}g'^{2}h^{4}\right], \qquad \gamma_{h \to SS} = \frac{1}{2}\left[(g^{2} + g'^{2})(\frac{11}{6}T^{2} + \frac{1}{4}h^{2})^{2} + \frac{1}{4}g^{2}g'^{2}h^{4}\right], \qquad \gamma_{h \to SS} = \frac{1}{2}\left[(g^{2} + g'^{2})(\frac{11}{6}T^{2} + \frac{1}{4}h^{2})^{2} + \frac{1}{4}g^{2}g'^{2}h^{4}\right], \qquad \gamma_{h \to SS} = \frac{1}{2}\left[(g^{2} + g'^{2})(\frac{11}{6}T^{2} + \frac{1}{4}h^{2})^{2} + \frac{1}{4}g^{2}g'^{2}h^{4}\right], \qquad \gamma_{h \to SS} = \frac{1}{2}\left[(g^{2} + g'^{2})(\frac{11}{6}T^{2} + \frac{1}{4}h^{2})^{2} + \frac{1}{4}g^{2}g'^{2}h^{4}\right], \qquad \gamma_{h \to SS} = \frac{1}{2}\left[(g^{2} + g'^{2})(\frac{11}{6}T^{2} + \frac{1}{4}h^{2})^{2} + \frac{1}{4}g^{2}g'^{2}h^{4}\right], \qquad \gamma_{h \to SS} = \frac{1}{2}\left[(g^{2} + g'^{2})(\frac{11}{6}T^{2} + \frac{1}{4}h^{2})^{2} + \frac{1}{4}g^{2}g'^{2}h^{4}\right], \qquad \gamma_{h \to SS} = \frac{1}{2}\left[(g^{2} + g'^{2})(\frac{11}{6}T^{2} + \frac{1}{4}h^{2})^{2} + \frac{1}{4}g^{2}g'^{2}h^{4}\right], \qquad \gamma_{h \to SS} = \frac{1}{2}\left[(g^{2} + g'^{2})(\frac{11}{6}T^{2} + \frac{1}{4}h^{2})^{2} + \frac{1}{4}g^{2}g'^{2}h^{4}\right], \qquad \gamma_{h \to SS} = \frac{1}{2}\left[(g^{2} + g'^{2})(\frac{11}{6}T^{2} + \frac{1}{4}h^{2})^{2} + \frac{1}{4}g^{2}g'^{2}h^{4}\right], \qquad \gamma_{h \to SS} = \frac{1}{2}\left[(g^{2} + g'^{2})(\frac{11}{6}T^{2} + \frac{1}{4}h^{2})^{2} + \frac{1}{4}g^{2}g'^{2}h^{4}\right], \qquad \gamma_{h \to SS} = \frac{1}{2}\left[(g^{2} + g'^{2})(\frac{11}{6}T^{2} + \frac{1}{4}h^{2})^{2} + \frac{1}{4}g^{2}g'^{2}h^{4}\right], \qquad \gamma_{h$$

Appendix C: Decay widths

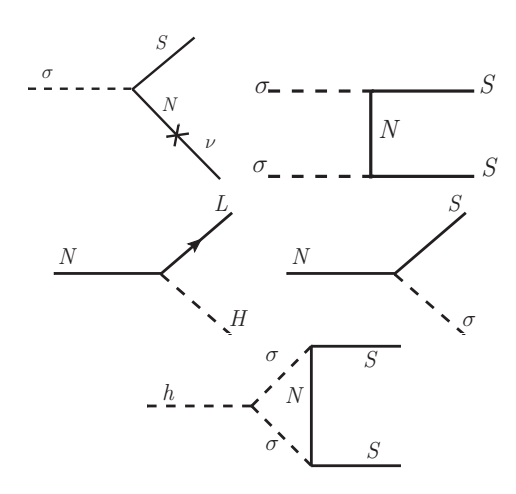


FIG. 13. DM production from σ decay (top left), h decay (bottom), $\sigma\sigma$ annihilation (top right), N decay (middle right). DM can thermalized via $\sigma\sigma \to SS$ channel. Leptogenesis production from N decay (middle left).

The different decay widths for the processes shown in Fig. 13 are given as

$$\Gamma_{N_1 \to LH} = \frac{(y^{\dagger}y)_{11}}{8\pi} m_{N_1}$$
(C1)

$$\Gamma_{N \to \sigma S} = \frac{y_{NS}^2}{16\pi m_{N_1}^3} \left((m_{N_1} + m_S)^2 - m_{\sigma}^2 \right)$$

$$\sqrt{m_{\sigma}^4 + (m_{N_1}^2 - m_S^2)^2 - 2m_{\sigma}^2 (m_{N_1}^2 + m_S^2)}$$
(C2)

$$\Gamma_{\sigma \to S\nu} = \frac{m_{\sigma}}{32\pi} \frac{y_{NS}^2 y^2 v_h^2}{m_{N_1}^2} \left(1 - \frac{m_s^2}{m_{\sigma}^2} \right)^2$$
 (C3)

$$\Gamma_{h \to SS} = \frac{y_{\text{eff}}^2}{16\pi} m_h \left(1 - \frac{4m_S^2}{m_h^2} \right)^{3/2},$$
(C4)

$$y_{\text{eff}} = \frac{y_{NS}^2 \lambda_{h\sigma} m_{N_1} v_h \mathcal{C}_0[m_h^2, m_S^2, m_S^2, m_{\sigma}, m_{\sigma}, m_{N_1}]}{4\sqrt{2}\pi^2},$$
(C5)

The thermally averaged decay widths are given as

$$\langle \Gamma_{\sigma} \rangle = \Gamma_{\sigma} \frac{K_1(m_{\sigma}/T)}{K_2(m_{\sigma}/T)}$$

$$\langle \Gamma_h \rangle = \Gamma_h \frac{K_1(m_h/T)}{K_2(m_h/T)}$$
(C6)

Appendix D: Thermally averaged cross-sections

We calculate the cross-sections using Calcher [42]. The thermally averaged cross-sections are then given as

$$\langle \sigma v \rangle_{ab \to cd} = \frac{T}{32\pi^4} \frac{g_a g_b}{n_a^{\text{eq}} n_b^{\text{eq}}} \int_{\max[(m_a + m_b)^2, (m_c + m_d)^2]}^{\infty} ds$$
$$\sigma(s) \frac{\left[(s - m_a - m_b)^2 - 4m_a^2 m_b^2 \right]}{\sqrt{s}} K_1(\frac{\sqrt{s}}{T})$$
(D1)

Appendix E: Direct detection of dark matter

The DM can scatter off with the target nucleus via a one-loop diagram as shown in Fig. 14. The effective coupling between the DM and the SM Higgs can be written from Fig. 14 as

$$y_{hSS}^{\text{eff}} = \frac{y_{NS}^2 \lambda_{h\sigma} v_h m_{N_1}}{8\sqrt{2}\pi^2 m_S} \left[\log \left(\frac{m_{N_1}^2}{m_{\sigma}^2} \right) - \frac{2\mathcal{A}}{\sqrt{\mathcal{BC}}} \log \left(\frac{\mathcal{A} - 2m_{N_1}^2 + \sqrt{\mathcal{BC}}}{2m_{N_1} m_{\sigma}} \right) \right], \text{ (E1)}$$

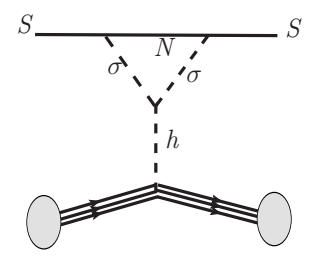


FIG. 14. Feynman Diagram for spin-independent DM-nucleon scattering at one loop.

where
$$\mathcal{A} = m_{N_1}^2 + m_S^2 - m_{\sigma}^2$$
, $\mathcal{B} = (m_{N_1} + m_{\sigma})^2 - m_S^2$, $\mathcal{C} = (m_{N_1} - m_{\sigma})^2 - m_S^2$.

The spin-independent cross-section is given as

$$\sigma_{\rm DM-N}^{\rm SI} = \frac{\mu^2}{\pi A^2} \mathcal{M}^2 \tag{E2}$$

were μ is the reduced mass of the DM-nucleon system, A is the mass number of the target nucleus, and \mathcal{M} is the amplitude of the diagram shown in Fig. 14 and is given

as

$$\mathcal{M} = Z * f_p + (A - Z) * f_n, \tag{E3}$$

with Z being the atomic number and interaction strengths between the DM and proton, neutron are given as

$$f_{p} = \sum_{q \in u,d,s} f_{p}^{q} \alpha^{q} \frac{m_{p}}{m_{q}} + \frac{2}{27} \sum_{Q \in c,b,t} f_{p}^{Q} \alpha^{Q} \frac{m_{p}}{m_{Q}},$$

$$f_{n} = \sum_{q \in u,d,s} f_{n}^{q} \alpha^{q} \frac{m_{n}}{m_{q}} + \frac{2}{27} \sum_{Q \in c,b,t} f_{n}^{Q} \alpha^{Q} \frac{m_{n}}{m_{Q}}, \quad (E4)$$

where

$$\alpha^{q} = y_{hSS}^{\text{eff}} \frac{m_{q}}{v_{h}} \frac{1}{m_{h}^{2}}, \ \alpha^{Q} = y_{hSS}^{\text{eff}} \frac{m_{Q}}{v_{h}} \frac{1}{m_{h}^{2}}.$$
 (E5)

Now we compute the direct detection cross-section taking two point from the left panel of Fig. 11 as $\{m_S = 1 \text{ MeV}, y_{\text{eff}} = 5.5 \times 10^{-10}\}$, and $\{m_S = 62 \text{ GeV}, y_{\text{eff}} = 4 \times 10^{-11}\}$. The cross-sections for these two points are $2.78 \times 10^{-67} \text{ cm}^2$ and $1.26 \times 10^{-63} \text{ cm}^2$, respectively. These are well below the current constraints on the spin-independent cross-section from the LZ [43] experiment or the future sensitivity of DARWIN [44].

- [1] P. Minkowski, $\mu \to e \gamma$ at a Rate of One Out of 10^9 Muon Decays?, Phys. Lett. B **67**, 421 (1977).
- [2] M. Gell-Mann, P. Ramond, and R. Slansky, Complex Spinors and Unified Theories, Conf. Proc. C 790927, 315 (1979), arXiv:1306.4669 [hep-th].
- [3] R. N. Mohapatra and G. Senjanovic, Neutrino Mass and Spontaneous Parity Nonconservation, Phys. Rev. Lett. 44, 912 (1980).
- [4] J. Schechter and J. W. F. Valle, Neutrino Masses in SU(2)x U(1) Theories, Phys. Rev. D 22, 2227 (1980).
- [5] E. Ma, Derivation of Dark Matter Parity from Lepton Parity, Phys. Rev. Lett. 115, 011801 (2015), arXiv:1502.02200 [hep-ph].
- [6] E. Ma, Light dark fermion in two natural scenarios, Nucl. Phys. B 1010, 116761 (2025), arXiv:2409.16246 [hep-ph].
- [7] E. Ma, P. K. Paul, and N. Sahu, Lepton parity dark matter and naturally unstable domain walls, Phys. Rev. D 112, 095020 (2025), arXiv:2508.02642 [hep-ph].
- [8] D. Curtin, P. Meade, and C.-T. Yu, Testing Electroweak Baryogenesis with Future Colliders, JHEP 11, 127, arXiv:1409.0005 [hep-ph].
- [9] U. K. Dey, S. K. Manna, P. K. Paul, S. K. Sahoo, and N. Sahu, Gravitational Wave Probe of Singlet-Doublet Dark Matter Induced Radiative Neutrino Mass, (2025), arXiv:2511.19386 [hep-ph].
- [10] A. G. Adame et al. (DESI), DESI 2024 VI: cosmological constraints from the measurements of baryon acoustic oscillations, JCAP 02, 021, arXiv:2404.03002 [astro-ph.CO].
- [11] N. Aghanim et al. (Planck), Planck 2018 results. VI. Cosmological parameters, Astron. Astrophys. 641, A6

- (2020), [Erratum: Astron.Astrophys. 652, C4 (2021)], arXiv:1807.06209 [astro-ph.CO].
- [12] E. Calabrese et al. (ACT), The Atacama Cosmology Telescope: DR6 Constraints on Extended Cosmological Models, (2025), arXiv:2503.14454 [astro-ph.CO].
- [13] J. S. Avva et al. (SPT-3G), Particle Physics with the Cosmic Microwave Background with SPT-3G, J. Phys. Conf. Ser. 1468, 012008 (2020), arXiv:1911.08047 [astro-ph.CO].
- [14] K. Abazajian et al., CMB-S4 Science Case, Reference Design, and Project Plan, (2019), arXiv:1907.04473 [astro-ph.IM].
- [15] S. Aiola et al. (CMB-HD), Snowmass2021 CMB-HD White Paper, (2022), arXiv:2203.05728 [astro-ph.CO].
- [16] A. Falkowski, J. T. Ruderman, and T. Volansky, Asymmetric Dark Matter from Leptogenesis, JHEP 05, 106, arXiv:1101.4936 [hep-ph].
- [17] D. Borah, S. Mahapatra, P. K. Paul, N. Sahu, and P. Shukla, Asymmetric self-interacting dark matter with a canonical seesaw model, Phys. Rev. D 110, 035033 (2024), arXiv:2404.14912 [hep-ph].
- [18] S. Mahapatra, P. K. Paul, N. Sahu, and P. Shukla, Asymmetric long-lived dark matter and leptogenesis from the type-III seesaw framework, Phys. Rev. D 111, 015043 (2025), arXiv:2305.11138 [hep-ph].
- [19] C. L. Wainwright, CosmoTransitions: Computing Cosmological Phase Transition Temperatures and Bubble Profiles with Multiple Fields, Comput. Phys. Commun. 183, 2006 (2012), arXiv:1109.4189 [hep-ph].
- [20] E. G. Adelberger, N. A. Collins, and C. D. Hoyle, Analytic expressions for gravitational inner multipole mo-

- ments of elementary solids and for the force between two rectangular solids, Class. Quant. Grav. 23, 125 (2006), [Erratum: Class.Quant.Grav. 23, 5463 (2006), Erratum: Class.Quant.Grav. 38, 059501 (2021)], arXiv:gr-qc/0512055.
- [21] N. Yunes and E. Berti, Accuracy of the post-Newtonian approximation: Optimal asymptotic expansion for quasicircular, extreme-mass ratio inspirals, Phys. Rev. D 77, 124006 (2008), [Erratum: Phys.Rev.D 83, 109901 (2011)], arXiv:0803.1853 [gr-qc].
- [22] S. Kawamura et al., Current status of space gravitational wave antenna DECIGO and B-DECIGO, PTEP 2021, 05A105 (2021), arXiv:2006.13545 [gr-qc].
- [23] K. Yagi and N. Seto, Detector configuration of DE-CIGO/BBO and identification of cosmological neutron-star binaries, Phys. Rev. D 83, 044011 (2011), [Erratum: Phys.Rev.D 95, 109901 (2017)], arXiv:1101.3940 [astro-ph.CO].
- [24] P. Amaro-Seoane et al. (LISA), Laser Interferometer Space Antenna, (2017), arXiv:1702.00786 [astro-ph.IM].
- [25] A. Sesana *et al.*, Unveiling the gravitational universe at μ -Hz frequencies, Exper. Astron. **51**, 1333 (2021), arXiv:1908.11391 [astro-ph.IM].
- [26] J. McDonald, Thermally generated gauge singlet scalars as selfinteracting dark matter, Phys. Rev. Lett. 88, 091304 (2002), arXiv:hep-ph/0106249.
- [27] J. McDonald and N. Sahu, keV Warm Dark Matter via the Supersymmetric Higgs Portal, Phys. Rev. D 79, 103523 (2009), arXiv:0809.0247 [hep-ph].
- [28] L. J. Hall, K. Jedamzik, J. March-Russell, and S. M. West, Freeze-In Production of FIMP Dark Matter, JHEP 03, 080, arXiv:0911.1120 [hep-ph].
- [29] G. Mangano, G. Miele, S. Pastor, T. Pinto, O. Pisanti, and P. D. Serpico, Relic neutrino decoupling including flavor oscillations, Nucl. Phys. B 729, 221 (2005), arXiv:hep-ph/0506164.
- [30] E. Grohs, G. M. Fuller, C. T. Kishimoto, M. W. Paris, and A. Vlasenko, Neutrino energy transport in weak decoupling and big bang nucleosynthesis, Phys. Rev. D 93, 083522 (2016), arXiv:1512.02205 [astro-ph.CO].
- [31] P. F. de Salas and S. Pastor, Relic neutrino decoupling with flavour oscillations revisited, JCAP 07, 051, arXiv:1606.06986 [hep-ph].
- [32] A. Biswas, D. Borah, N. Das, and D. Nanda, Freeze-in

- dark matter via a light Dirac neutrino portal, Phys. Rev. D 107, 015015 (2023), arXiv:2205.01144 [hep-ph].
- [33] D. Borah, S. Mahapatra, N. Sahu, and V. S. Thounaojam, Self-interacting dark matter with observable ΔNeff, Phys. Rev. D 112, 035037 (2025), arXiv:2504.16910 [hepph].
- [34] A. Pilaftsis and T. E. J. Underwood, Resonant leptogenesis, Nucl. Phys. B 692, 303 (2004), arXiv:hepph/0309342.
- [35] E. Nardi, Y. Nir, J. Racker, and E. Roulet, On Higgs and sphaleron effects during the leptogenesis era, JHEP 01, 068, arXiv:hep-ph/0512052.
- [36] S. Blanchet, P. Di Bari, D. A. Jones, and L. Marzola, Leptogenesis with heavy neutrino flavours: from density matrix to Boltzmann equations, JCAP 01, 041, arXiv:1112.4528 [hep-ph].
- [37] K. Moffat, S. Pascoli, S. T. Petcov, H. Schulz, and J. Turner, Three-flavored nonresonant leptogenesis at intermediate scales, Phys. Rev. D 98, 015036 (2018), arXiv:1804.05066 [hep-ph].
- [38] M. D'Onofrio, K. Rummukainen, and A. Tranberg, Sphaleron Rate in the Minimal Standard Model, Phys. Rev. Lett. 113, 141602 (2014), arXiv:1404.3565 [hep-ph].
- [39] A. De Simone and A. Riotto, On Resonant Leptogenesis, JCAP 08, 013, arXiv:0705.2183 [hep-ph].
- [40] P. Huang and K. Zhang, Testable flavored TeV-scale resonant leptogenesis with MeV-GeV dark matter in a neutrinophilic two-Higgs-doublet model, Phys. Rev. D 111, 115011 (2025), arXiv:2411.18973 [hep-ph].
- [41] W. Buchmuller, P. Di Bari, and M. Plumacher, Leptogenesis for pedestrians, Annals Phys. 315, 305 (2005), arXiv:hep-ph/0401240.
- [42] A. Belyaev, N. D. Christensen, and A. Pukhov, CalcHEP 3.4 for collider physics within and beyond the Standard Model, Comput. Phys. Commun. 184, 1729 (2013), arXiv:1207.6082 [hep-ph].
- [43] J. Aalbers et al. (LZ), Dark Matter Search Results from 4.2 Tonne-Years of Exposure of the LUX-ZEPLIN (LZ) Experiment, Phys. Rev. Lett. 135, 011802 (2025), arXiv:2410.17036 [hep-ex].
- [44] J. Aalbers et al. (DARWIN), DARWIN: towards the ultimate dark matter detector, JCAP 11, 017, arXiv:1606.07001 [astro-ph.IM].